ACS OMEGA

http://pubs.acs.org/journal/acsodf

Article

Tridimensional N, P-Codoped Carbon Sponges as Highly Selective Catalysts for Aerobic Oxidative Coupling of Benzylamine

Lu Peng,[§] Herme G. Baldovi,[§] Amarajothi Dhakshinamoorthy, Ana Primo,* and Hermenegildo Garcia*

Cite This: *ACS Omega* 2022, 7, 11092−11100

Read Online

ACCESS | Metrics & More | Article Recommendations | Supporting Information

ABSTRACT: Two tridimensional N-doped porous carbon sponges (3DC-X) have been prepared by using cetyltrimethylammonium chloride (CTAC) and cetyltrimethylammonium bromide (CTAB) as soft templates and alginate to replicate the liquid crystals formed by CTA^+ in water. Alginate is a filmogenic polysaccharide of natural origin having the ability to form nanometric defectless films around objects. Subsequent pyrolysis at 900 °C under an Ar flow of the resulting CTA^+−polysaccharide assemblies result in 3DC-1 and 3DC-2, with the N percentages of 0.48 and 0.36 wt % for the materials resulting from CTAC and CTAB, respectively. Another four 3DC materials were obtained via pyrolysis of the adduct of phytic acid and chitosan, rendering an amorphous, N and P-codoped carbon sample (3DC-3 to 3DC-6). The six 3DC samples exhibit a large area (>650 $m^2 \times g^{-1}$) and porosity, as determined by Ar adsorption. The catalytic activity of these materials in promoting the aerobic oxidation of benzylamine increases with the specific surface area and doping, being the largest for 3DC-4, which is able to achieve 73% benzylamine conversion to *N*-benzylidene benzylamine in solventless conditions at 70 °C in 5 h. Quenching studies and hot filtration tests indicate that 3DC-4 acts as a heterogeneous catalyst rather than an initiator, triggering the formation of hydroperoxyl and hydroxyl radicals as the main reactive oxygen species involved in the aerobic oxidation.

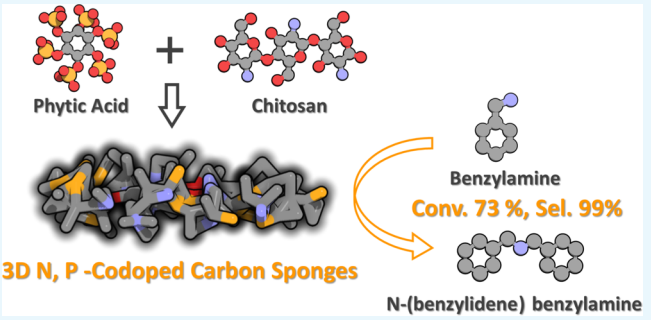

INTRODUCTION

Heterogeneous catalysis are currently dominated by the use of transition metals, most of them precious or critical metals, as active sites.[1,2] For the sake of sustainability, there is a current interest in catalysis to develop metal-free materials as alternative catalysts for metals.[3,4] Since graphene and related materials have become widely available, and considering the relevance that active carbons have had in catalysis, there has been considerable interest in exploiting the properties of defective graphenes as catalysts.[5−8] The ideal structure of graphene as a monoatom-thick 2D layer constituted by sp^2 carbons in a hexagonal geometry allows the generation of defects that can become active sites for different reactions such as aerobic oxidations and hydrogenations.[9,10] Among them, considering the greenness of using ambient oxygen as the terminal oxidant, oxidation of hydrocarbons, alcohols, and amines are particularly important.[11−14]

One of the main advantages of fully exfoliated, ideal graphene is its large surface area. In order to reduce the footprint of graphene materials, particularly for their applications in catalysis and electrocatalysis, one current line of research is to develop 3D graphene sponges in which a single layer or a few layers of graphenes become the walls of 3D structured porous carbonaceous materials.[15,16] Considering the importance of porosity in the activation of substrates due to confinement effects, as well as product selectivity due to steric constraints, it is also of interest to determine the activity of these 3D graphenes and related large-area porous carbons, with an area of over 1000 $m^2 \times g^{-1}$, as heterogeneous catalysts.[17,18]

Besides 3D structuring of carbon materials, doping by introducing heteroatoms in the solid network is a powerful strategy to generate active sites. The presence of nitrogen, sulfur, and other heteroatoms substantially increases the activity of the resulting doped carbons as oxidation catalysts.[19−22] Doping and codoping of graphitic carbons have also been used to develop electrocatalysts and in advanced battery materials.[23,24]

Considering the current interest of porous 3D carbon sponges and doped carbons, the combination of the two features in the same material could render even more efficient metal-free catalysts for aerobic oxidation. In this context, the present study reports the catalytic activity of porous N-doped 3D graphene samples (3DC-1 and 3DC-2) and porous N, P-

Received: December 20, 2021
Accepted: February 18, 2022
Published: March 25, 2022

codoped 3D carbon samples (3DC-4 to 3DC-6) as metal-free catalysts for the oxidative coupling of benzylamine (**1**) to *N*-(benzylidene)benzylamine (**2**). This reaction is useful in organic synthesis for the preparation of secondary symmetric amines, and the reaction has been proposed by Loh and co-workers as a benchmark aerobic oxidation to compare the catalytic activities of graphene oxide and carbon materials.[25,26] 3D carbon sponges co-doped by N and P exhibit an enhanced catalytic activity for the conversion of **1** into **2**, a performance that can be attributed to the combination of codoping, porosity, and the large surface area.

EXPERIMENTAL SECTION

Sample Preparation. Commercially available reagents were purchased from Aldrich and used without further purification.

Synthesis of 3DC-1 and 3DC-2. For the preparation of 3DC-1, 100 mg of sodium alginate from Aldrich and 0.4 mL of 25 wt % cetyltrimethylammonium chloride (CTAC) aqueous solution were dissolved in 80 and 20 mL of Milli-Q H_2O, respectively. After 2 h of magnetic stirring at room temperature, the CTAC aqueous solution was slowly added into the aqueous solution of sodium alginate under magnetic stirring. The mixed solution was further stirred for 6 h at room temperature. Then, the solution was transferred to a Teflon-lined autoclave and heated at 100 °C under autogenous pressure for 24 h. Afterward, water was evaporated at a low temperature of 60 °C. To obtain 3DC-1, the solid precursor resulting from the assembly of CTAC and sodium alginate was pyrolyzed under an Ar flow (200 mL min^{-1}), increasing the temperature at a rate of 5 °C min^{-1} up to 150 °C and then at 1 °C min^{-1} up to 900 °C, followed by a holding time of 2 h. For the synthesis of 3DC-2, 2 g of cetyltrimethylammonium bromide (CTAB) was added into 20 mL of Milli-Q water. After CTAB was dissolved completely at 60 °C, 2 g of sodium alginate was added into the CTAB solution under strong stirring at room temperature. The mixed solution was further stirred for 6 h at room temperature. Then, the solution was transferred to a Teflon-lined autoclave and heated at 100 °C under autogenous pressure for 24 h. Afterward, the autoclave was cooled down to room temperature, and the mixed solution was introduced dropwise, using a syringe (0.8 mm diameter needle), in an aqueous solution of calcium chloride (0.24 M, 300 mL). The gel microspheres were formed and immersed in $CaCl_2$ solution for 1 h and then profusely washed with distilled water. The resulting hydrogel microspheres were dehydrated by a series of ethanol/water baths with an increasing concentration of ethanol (10, 30, 50, 70, 90, and 100 vol %, respectively) for 15 min in each and stored in anhydrous ethanol. Template CTAB was removed from these spheres via solvent extraction in a mixed solution of ethanol (180 mL) and concentrated HCl (240 μL, 37 wt %). After that, the alcogel microspheres were washed with anhydrous ethanol (100 mL × 3) and exchanged by supercritical CO_2. To obtain 3DC-2, the dried spheres were pyrolyzed under an Ar flow (200 mL min^{-1}), while increasing the temperature at a rate of 5 °C min^{-1} up to 150 °C and then at 1 °C min^{-1} up to 900 °C, followed by maintaining the temperature for 2 h.

Synthesis of 3DC-3 to 3DC-6. In a general preparation, a certain volume of 50 wt % aqueous solution of phytic acid from Aldrich was diluted in 20 mL of Milli-Q water. After 1 h of magnetic stirring at room temperature, a certain quantity of chitosan was added slowly under stirring into the aqueous solution of phytic acid. The specific amounts of phytic acid and chitosan are shown in Table S1. The mixed solution was stirred overnight at room temperature. A solid containing the mixture of phytic acid and chitosan was obtained by water evaporation. To prepare 3DC-3 to 3DC-6, this mixture was pyrolyzed under an Ar flow (200 mL min^{-1}), while increasing the temperature at a rate of 5 °C min^{-1} up to 900 °C, followed by a holding time for 2 h. The resulting 3DC-3 to 3DC-6 samples were allowed to cool at room temperature under an Ar flow.

Sample Characterization. Raman spectra were collected using a Horiba Jobin Yvon LabRAM HR UV−visible−near-infrared (200−1600 nm) Raman microscope spectrometer using a 512 nm laser as the excitation source. The spectra were collected by averaging 10 scans at a resolution of 2 cm^{-1}. X-ray photoelectron spectroscopy (XPS) spectra were measured on a SPECS spectrometer equipped with a Phoibos 150 9MCD detector using a nonmonochromatic X-ray source (Al and Mg) operating at 200 W. The samples were evacuated in the prechamber of the spectrometer at 1 × 10^{-9} mbar. The measured intensity ratios of the components were obtained from the area of the corresponding peaks after nonlinear Shirley-type background subtraction and corrected using the response function of the spectrometer. The chemical composition of the samples was determined using combustion chemical analysis by using a CHNS FISONS elemental analyzer. The micropore volume and specific surface area of the solids were measured through Ar adsorption isotherms at −186 °C by using a Micromeritics ASAP 2020 instrument. Field emission scanning electron microscopy (FESEM) images were acquired by using a JEOL JSM 6300 apparatus. High-resolution transmission electron microscopy (HRTEM) images were recorded on a JEOL JEM 2100F under an accelerating voltage of 200 kV. Samples were prepared by applying one drop of the suspended material in ethanol onto a carbon-coated nickel TEM grid and allowing them to dry at room temperature.

Catalytic Tests. Reactions of benzylamine oxidation were carried out by previously activating 10 mg of the catalyst in a round-bottom flask at 120 °C in a vacuum for 24 h. Then, the activated catalyst was placed into a 25 mL two-neck round-bottom flask, followed by the addition of benzylamine (freshly purified by redistillation, ≥99.5%, Merck, 100 μL) in 3 mL of acetonitrile and sonication for 15 min. The reaction mixture was vigorously stirred, heated to 70 °C, and purged with an oxygen flow (purity 99.999%, 0.25 L·min^{-1}) at atmospheric pressure. Aliquots were periodically taken at the appropriate time and diluted in a chloroform solution containing a known amount of nitrobenzene as an external standard. The samples were immediately analyzed via gas chromatography (GC) using a flame ionization detector. Quantification was carried out based on calibration plots considering the response factor and the relative peak areas. During reusability tests, the catalyst was recovered at the end of the reaction through filtration with a polytetrafluoroethylene filter with a 0.2 μm pore diameter. The catalyst was washed and recovered from the filter with chloroform, and the solvent was removed from the flask, where the subsequent reaction was going to take place.

Reusability Test. The reaction for the reusability test was repeated following the same reaction conditions but only lasting for 3 h. After each reaction, the catalyst was recovered by centrifuging at 10 000 rpm for 10 min and washed with acetonitrile four times. The solid was taken up with 5 mL of acetonitrile and placed in a 25 mL two-neck round-bottom

https://doi.org/10.1021/acsomega.1c07179
ACS Omega 2022, 7, 11092−11100

Scheme 1. (a) Illustration of the Formation of 3DC-1 and 3DC-2 Based on the Use of CTA^+ as a Soft Template: (i) Hydrothermal Method; (ii) Solvent Evaporation; (iii) Polysaccharide Replication of CTA^+ Rods; and (iv) Pyrolysis in Ar and (b) Illustration of the Formation at the Nanoscale of 3DC-3 to 3DC-6: (i) Mixture of Phytic Acid and Chitosan and (ii) Pyrolysis in Ar

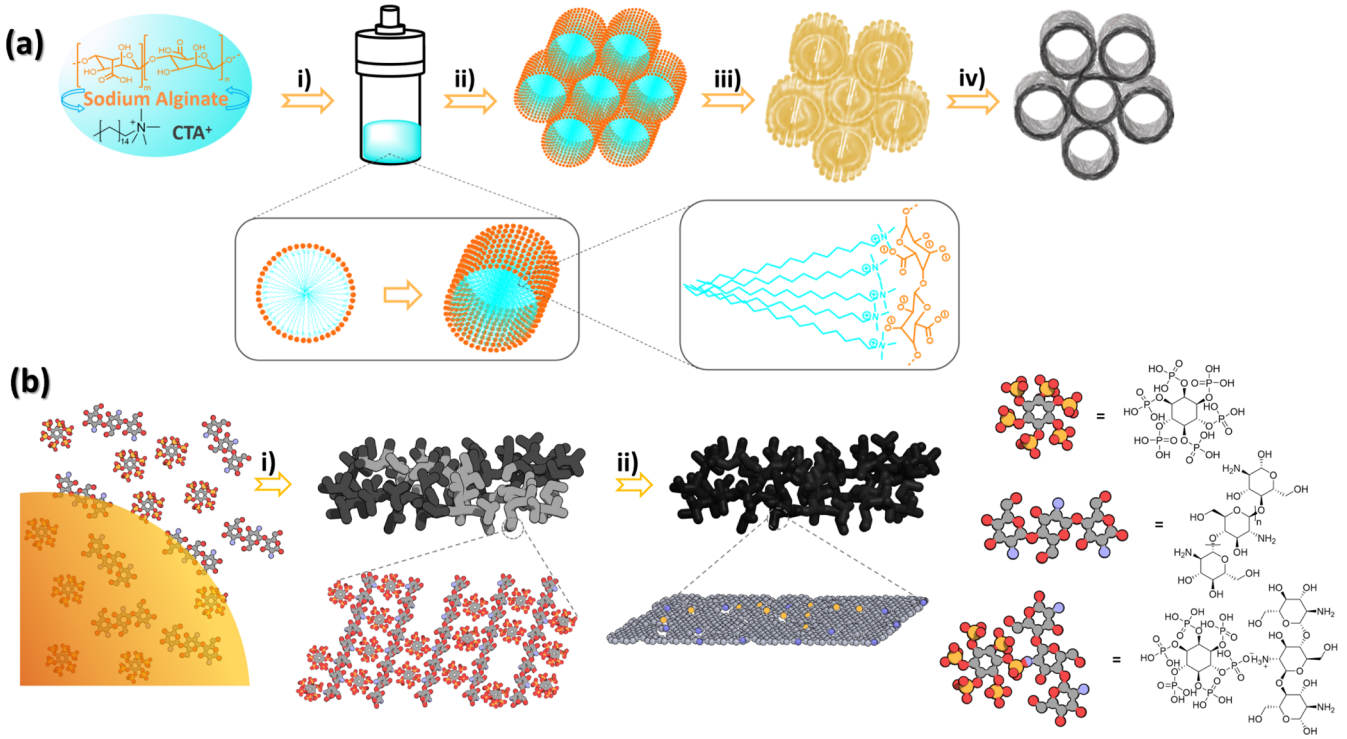

Table 1. Analytical Data, Specific Surface Area, and Porosity Values of the Materials Tested as Catalysts for the Oxidative Coupling of Benzylamine (1)

catalysts	C (wt %)[a]	N (wt %)[a]	P (wt %)[b]	molar ratio (P/N)	surface area (m^2/g)	micropore volume (cm^3/g)
3DC-1	85.19	0.48	0	0	887	0.29
3DC-2	62.59	0.36	0	0	819	0.23
3DC-3	66.52	4.43	1.33	0.14	665	0.32
3DC-4	64.22	3.02	1.35	0.20	734	0.34
3DC-5	58.58	1.45	5.99	1.87	1141	0.36
3DC-6	55.13	0.96	10.53	4.96	1249	0.43

[a]The residual percentage up to 100% is due to the presence of oxygen. [b]Determined using inductively coupled plasma atomic emission spectrometry analysis after dissolving the metals in aqua regia.

flask. Then, the solvent was completely evaporated to activate the catalyst at 130° C for 12 h in vacuum.

RESULTS AND DISCUSSION

Considering the novelty of the procedure to obtain these materials, the preparation of the tridirectional graphene sponges (3DC) is first described by providing characterization data about the porosity, surface area, and structure before reporting, in a subsequent section, their catalytic activity.

Preparation of 3D-C. A recent publication has disclosed the preparation of 3DC with hierarchically uniform porosity from mesopores to ultramicropores by using a soft-templating method.[27] Scheme 1a illustrates the preparation procedure for 3DC samples.

The process is based on the spontaneous self-assembly of cetyltrimethylammonium (CTA^+) and the ability of filmogenic sodium alginate to replicate the soft liquid crystal rods formed by CTA^+ aggregates. Alginate and other natural polysaccharides are known for their ability to form continuous, high-quality, thin films of subnanometric roughness conformal with the surface of rigid substrates.[28,29] The filmogenic property of certain polysaccharides is the reason why natural selection has resulted in the use of chitin as the universal biopolymer constituent of the skin of insects and crustaceans, thus reflecting the extremely high performance of this biopolymer to replicate objects and surfaces.[30] Previous studies have shown that chitosan, a polysaccharide of glucosamine, is a suitable precursor for defective nitrogen-doped graphene.[31,32] According to Scheme 1, the same ability to form conformal films should also be responsible for the formation of pores by an appropriate coating of positive CTA^+ self-assembled rods and negative alginate fibrils. In the present study, two different concentrations of CTA^+ chloride (CTAC) and CTA^+ bromide (CTAB) were used for the preparation of two samples, namely, 3DC-1 and 3DC-2, respectively.

Besides filmogenecity, polysaccharides also have the property to undergo graphitization upon pyrolysis at temperatures of around 900 °C or higher, thus rendering defective

https://doi.org/10.1021/acsomega.1c07179
ACS Omega 2022, 7, 11092−11100

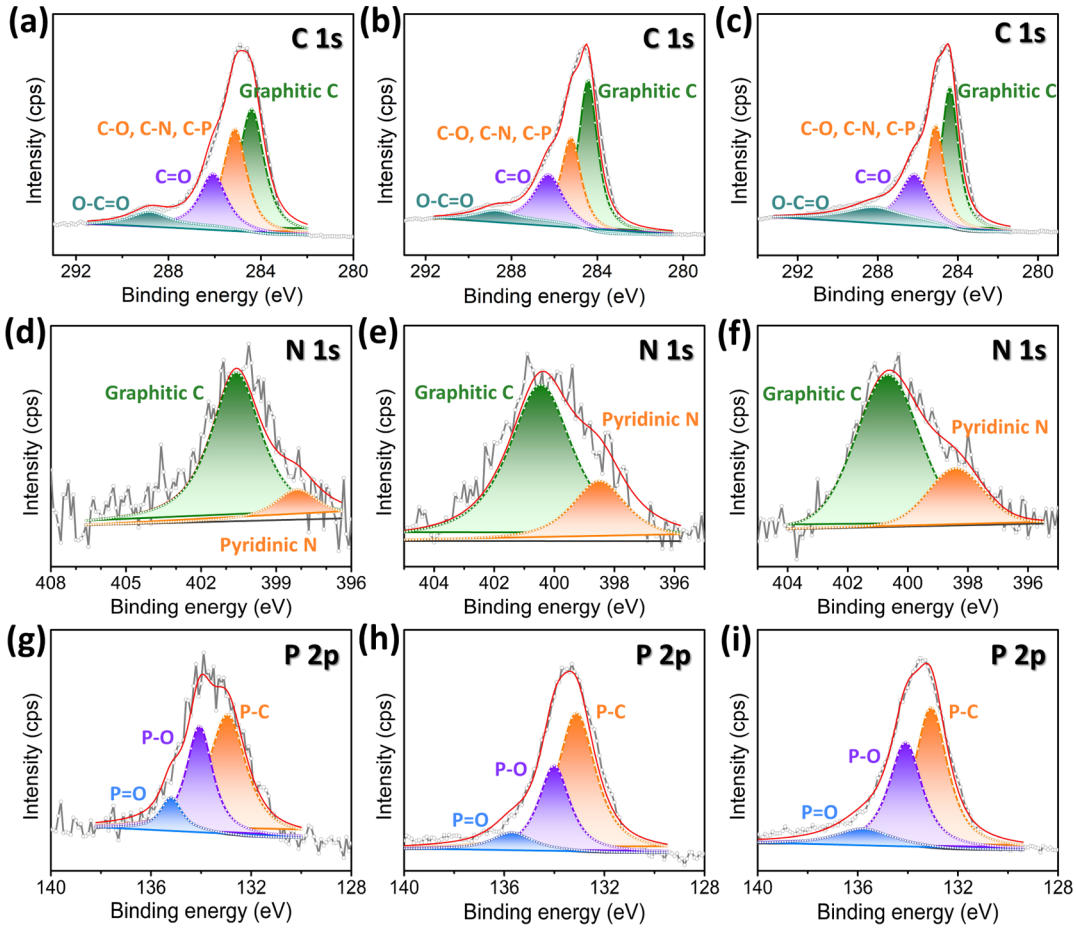

Figure 1. XPS spectra recorded for samples 3DC-4 (a,d,g), 3DC-5 (b,e,h), and 3DC-6 (c,f,i) and the best deconvolution to individual components (C 1s, N 1s, and P 2p).

graphene (step iv in Scheme 1a).[31] In the present case, since CTA^+, acting as a template, has provided a 3D structure to the sodium alginate precursor (steps ii and iii in Scheme 1a), the pyrolysis of this material renders defective 3D graphene sponges. Importantly, combustion chemical analysis after pyrolysis shows the incorporation of some amount of nitrogen (from the composition of CTA^+) as the dopant element in the resulting 3DC material. Table 1 summarizes the analytical values and adsorption isotherms of the 3DC materials under study.

Besides 3DC-1 and 3DC-2, the present study also includes a different type of tridimensional carbonaceous material obtained by the pyrolysis of the adduct with phytic acid and chitosan. The process is also summarized in Scheme 1b. Phytic acid upon pyrolysis renders a P-doped graphene, exhibiting activity for water reforming at moderate temperatures due to the high content of phosphorus as the dopant element.[33] The strategy, herein, has been to conjugate phytic acid and chitosan. Pyrolysis of the adduct with phytic acid and chitosan would render a 3D carbonaceous material simultaneously codoped with nitrogen and phosphorous. Table 1 summarizes the main analytical and textural data of 3DC-3 to 3DC-6 materials prepared in the present study. For the sake of comparison, the related metal-free carbonaceous catalysts were also studied to determine their relative efficiencies to promote the oxidative coupling of **1**. Specifically, the list of catalysts contains defective N-doped graphene [(N)G] obtained by pyrolysis of the chitosan aerogel, as well as commercial samples of active carbon and reduced graphene oxide (rGO).

The graphene structures of the six 3DC materials under study were ascertained using Raman spectroscopy (Figure S1), which for these new materials exhibit the characteristic 2D, G, and D peaks, appearing at 2700, 1590, and 1350 cm^{-1}, respectively. The broadness of the partially resolved G and D peaks and the relative intensities are in agreement with the defective nature of the 3D graphene materials with the presence of oxygenated functional groups and dopant elements. We notice, however, that upon increasing the percentage of phytic acid, the resulting 3D-4 to 3D-6 carbons exhibit a narrower G band and, particularly 3D-6, better resolved harmonic bands in the 3300−2500 cm^{-1} region. We propose that these changes observed in the Raman spectra associated to the improvement in the graphitic quality of the codoped material could be due to the beneficial effect of the acidity of the hydrogenphosphate groups during the pyrolysis favoring graphitization of the polysaccharide precursor.

XPS analysis of the 3DC materials confirmed the presence of O and N as dopant elements in 3DC materials. In addition, the presence of P was also detected. Figures 1 and S2 present the XPS spectra of samples 3DC-4 to 3DC-6 and 3DC-1 to 3DC-2, respectively, while Table S2 lists the components of each type of C, N, and P atoms. High-resolution XPS spectra of the C 1s peak (Figures 1a−c and S2a,b) can be in general deconvoluted for the 3DC materials into four main components, corresponding in various proportions to graphitic

https://doi.org/10.1021/acsomega.1c07179
ACS Omega 2022, 7, 11092−11100

carbon (284.5 eV), carbon bonded to nitrogen, oxygen or phosphorus through a single bond (285.1 eV), carbon bonded by a double bond to nitrogen or oxygen (286.3 eV), and the carboxyl group (288.5 eV), respectively. Also, for N atoms, the XPS N 1s spectra (Figures 1d–f and S2c,d) for 3DC samples can be deconvoluted into two different components at 400.0 and 398.3 eV, attributable to graphitic nitrogen and pyridinic nitrogen, respectively. These various nitrogen species can exhibit different catalytic activities, promoting different reactions.[19,34,35]

In the case of 3DC-4 to 3DC-6, analysis of the P 2p peak indicates the presence of three different types of phosphorous atoms, appearing at binding energy values of 133.1, 134.1, and 135.7 eV that are attributable to P–C, P–O, and P═O, respectively.

As can be seen, while the surface area of graphite is negligible, the surface area of the 3DC materials is considerably larger, more than 650 m^2/g. The specific surface area of 3DC-6 obtained by pyrolysis at 900 °C was initially measured using isothermal Ar adsorption, obtaining a value of 1249 $m^2 \times g^{-1}$ (Table 1). Gas adsorption measurements on solid samples of powdered graphene typically give much lower specific surface area values in the range of 100 $m^2 \times g^{-1}$ due to the stacking of the layers and reduced micro-/mesoporosity. In this regard, the specific surface area values measured for 3DC samples are remarkable and much larger than the reported values. On the other hand, Ar adsorption isotherms also indicate higher micropore volume values. Again, these micropores are remarkable and can have consequences on the catalytic activity due to the possible confinement effects that could take place when the reaction occurs in a constraint space.

FESEM shows that the 3DC materials are constituted by particles with dimensions of 100 and 200 nm. Figure 2 shows a selection of FESEM images to illustrate the morphology of the 3D samples under study. Of note is the fact that in contrast to the behavior of structured turbostratic graphitic carbons that undergo extensive exfoliation upon sonication, and as expected for particulate 3D materials, the present 3DC sponges maintain the particulate morphology without substantial exfoliation when they are subjected to extended periods of ultrasound (see Figure S3).

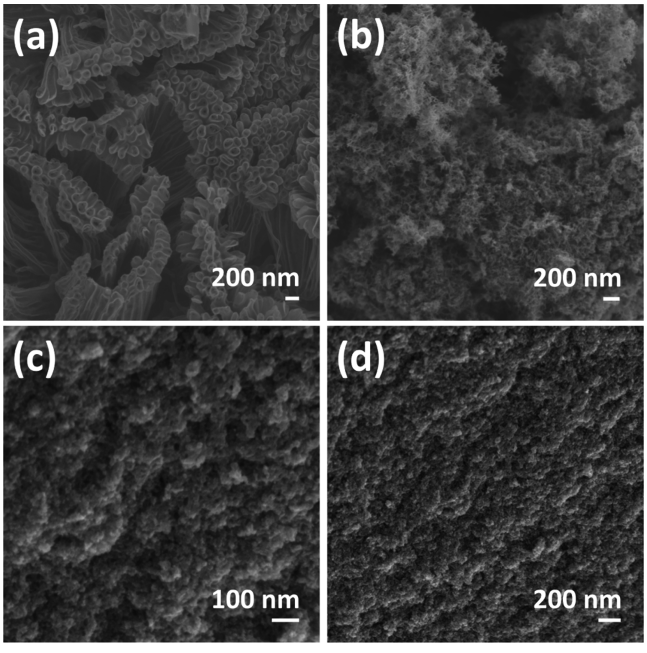

Figure 2. FESEM images of as-prepared 3DC-1 (a), 3DC-2, (b) and 3DC-4 (c,d).

The graphenic structure of 3DC-1 and 3DC-2 was ascertained using HRTEM, where upon magnification, the hexagonal arrangement of the layers can be observed, confirming the crystallinity of 3DC-1 and 3DC-2. In contrast, probably due to the different preparation procedure and the presence of P doping, 3DC-3 to 3DC-6 have a structure of amorphous carbon. Figure 3 shows some selected HRTEM images obtained for 3DC-1, 3DC-2, 3DC-4, and 3DC-6 samples under study, while Figure S4 compiles these for the other samples under study.

Catalytic Activity. As indicated in the Introduction section, the focus of the present study is to determine the influence of the 3D structure with the presence of pores together with the dopant on the activity as metal-free catalysts for the aerobic oxidation of benzylamine. The reaction under study is illustrated in eq 1, while Table 2 provides the results of

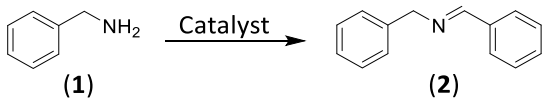

the screening of the catalytic activity of the materials under study.The above equation shows the oxidative coupling of benzylamine (**1**) to *N*-(benzylidene) benzylamine (**2**).

The control with the absence of any catalyst shows that the conversion of compound **1** into compound **2** occurs in a negligible percentage after 5 h of reaction time under the reaction conditions. In the case of (N)G obtained from the pyrolysis of the chitosan aerogel, the presence of nitrogen doping of 8.03 wt % significantly increases the formation of *N*-benzylidene amine, reaching a very high conversion of 44%. Sample 3DC-1 with a more defined porosity but an 0.48% amount of nitrogen exhibits an increase in catalytic activity, with the overall conversion of **1** being improved compared to that of (N)G. A 4-fold higher activity was observed for 3DC-2, which was considerably more active than rGO (Table 2, entry 11) in promoting the oxidative coupling of 1 to 2 with higher selectivity. It should be noted that for rGO, the nature of the active sites and the reaction intermediates could be different from those of 3DC-2. The higher activity of 3DC-1 than that of 3DC-2 can be attributed to the higher nitrogen content and specific surface area for 3DC-1 than that for 3DC-2 (see Table 1). The presence of phosphorous as a dopant can explain the higher activity observed for 3DC-3 to 3DC-6, among which 3DC-4 was the most active metal-free catalyst of the series, reaching the highest conversion of 73% and almost complete selectivity to product **2**. The temporal profile of benzylamine conversion in the presence of 3DC-3 to 3DC-6 with different molar ratios of P and N is shown in Figure 4. Overall, the catalytic data given in Table 2 show that carbonaceous materials lacking N or P, such as graphite or rGO, are less active and the presence of porosity enhances the activity of (N)G. This conclusion is in line with the current understanding of the influence of dopant elements and the surface area on the catalytic activity of graphenes and related materials.[3,4] While N atoms introduce efficient active sites, codoping with P further increases the activity of the resulting material, as observed in other examples. However, for the series of N, P-codoped 3D carbons, the catalytic activity does

https://doi.org/10.1021/acsomega.1c07179
ACS Omega 2022, 7, 11092–11100

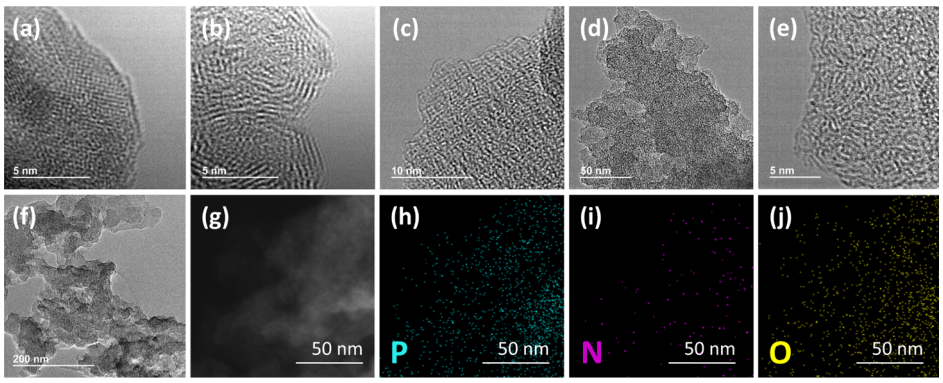

Figure 3. HRTEM images of 3DC-1 (a), 3DC-2 (b), 3DC-4 (c,d), and 3DC-6 (e,f) with corresponding energy-dispersive spectroscopy elemental mapping images (g–j). The elemental mapping images for P, N, and O show a uniform distribution of the elements.

Table 2. Results of the Aerobic Oxidation of Benzylamine (1) into *N*-(benzylidene) Benzylamine (2) in the Presence of Various Carbon-Based Catalysts[a]

entry	catalyst	conversion (%)[b]	selectivity (%)[b]
1	blank	≤1	99
2	(N)G	44	99
3	3DC-1	58	99
4	3DC-2	12	99
5	3DC-3	28	99
6	3DC-4	73	99
7	3DC-5	54	99
8	3DC-6	51	99
9	graphite	≤2	98
10	active carbon	7	98
11	rGO	3	97
12	3DC-4[c]	61	99
13	3DC-4[d]	49	99
14	3DC-4[e]	7	98
15	3DC-4[f]	27	99

[a]Reaction conditions: benzylamine (0.91 mmol, 100 μL) in acetonitrile (3 mL), catalyst (10 mg), oxygen purged (0.25 L·min^{-1}), 70 °C, 5 h. [b]Determined using GC. [c]Without a quencher, 3 h. [d]BHT (50 mg), 3 h. [e]DMSO (275 mg), 3 h. [f]TEMPO (50 mg), 3 h.

not correlate with a high population of the P dopant (higher for 3D-5 and 3D-6) or surface area (higher for 3D-5 or 3D-6) but seems to be a compromise of several factors, among which better graphitization (observed using Raman spectroscopy for 3D-4 to 3D-6) and an adequate N/P ratio (higher than 1 for 3D-3 and 3D-4) appear to also be contributing.

The stability of 3DC-4 was confirmed by performing four consecutive reuses of the recovered sample in a 3 h reaction. The catalyst was recovered at the end of the reaction by washing with acetonitrile four times and drying at 130 °C for 12 h under vacuum. The results presented in Figure 5 show that 3DC-4 with a P and N molar ratio of 0.2 is stable after being reused four times. Catalytic activity with a minor change could be due to the partial deactivation of the metal-free catalyst or the unavoidable loss of the catalyst in the reuse workup. In any case, the profile shown in Figure 5 indicates

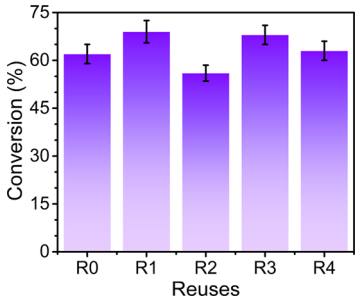

Figure 5. Conversion of benzylamine for 3DC-4 upon four consecutive reuses. Reaction conditions: benzylamine (0.91 mmol, 100 μL) in acetonitrile (3 mL), catalyst (10 mg), oxygen purged (0.25 L·min^{-1}), 70 °C, 3 h.

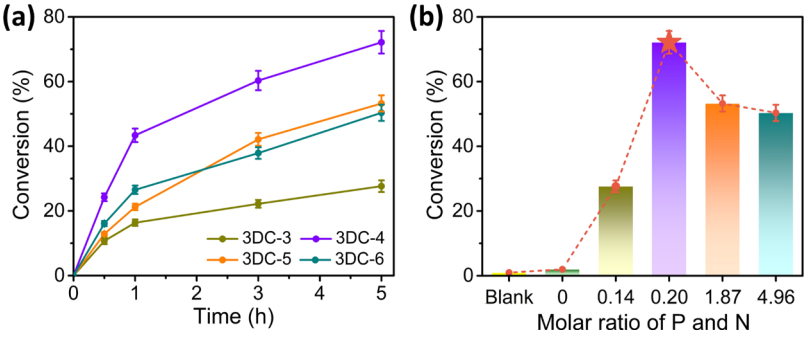

Figure 4. (a) Time conversion plot for the conversion of benzylamine in the presence of 3DC-3 to 3DC-6 and (b) conversion comparison of catalysts with different molar ratios of P and N. Reaction conditions: benzylamine (0.91 mmol, 100 μL) in acetonitrile (3 mL), catalyst (10 mg), oxygen purged (0.25 L·min^{-1}), 70 °C.

https://doi.org/10.1021/acsomega.1c07179
ACS Omega 2022, 7, 11092−11100

Scheme 2. Proposed Reaction Mechanism for the Oxidative Coupling of Benzylamine (1) to *N*-(Benzylidene) Benzylamine (2)

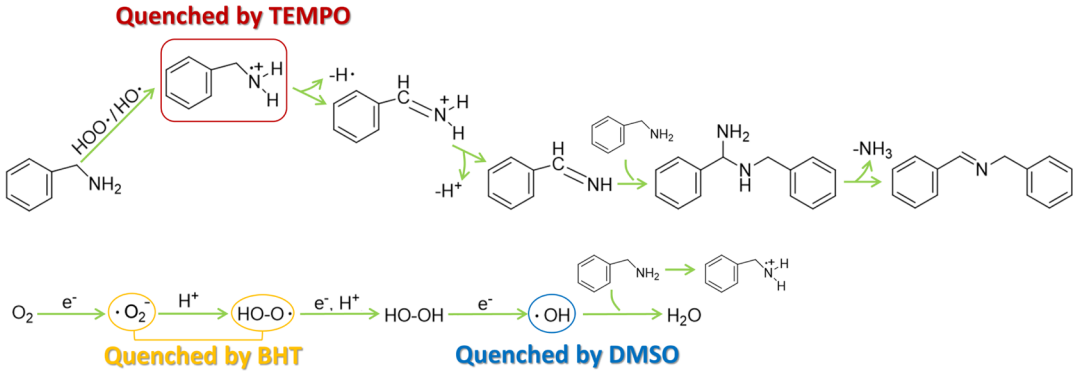

that 3DC-4 is a very stable metal-free catalyst for the oxidative coupling of compound **1**.

To understand the reactive oxygen species involved in the process, the reaction was carried out in the presence of butylated hydroxy toluene (BHT) and dimethyl sulfoxide (DMSO), which are typical quenchers for hydroperoxyl and hydroxyl radicals, respectively. The use of quenchers is a very powerful method to determine the nature of the main reactive oxygen species responsible for aerobic oxidations. According to Table 2 (entries 12−15), it is found that the use of radical quenchers or radical trapping agents can produce an appreciable impact on the reaction efficiency. BHT, which reacts with superoxide and hydroperoxyl radicals, produces a slight decrease in the overall benzylamine conversion, while DMSO inhibits nearly 60% of the conversion. In addition, (2,2,6,6-tetramethylpiperidin-1-yl)oxyl (TEMPO) seems to be an effective quencher, stopping the reaction almost completely. All these facts together indicate that most of the catalytic activity is initiated by the formation of hydroxyl radicals that can be quenched by DMSO. First, hydroxyl radicals are produced from the prior formation of the superoxide via electron transfer from the electron donor functional groups present into the carbon sponges or the amine of the benzylamine reactant itself. Based on the negligible conversion of benzylamine in the absence of the catalyst, it can be concluded that graphitic sponge is mainly responsible for the activation of oxygen and the formation of hydroxyl radicals. Hydroxyl radicals will form benzyl radicals either via direct benzylic hydrogen abstraction or through the intermediacy of an aminium radical cation, followed by deprotonation at the benzylic position. One plausible reason for incomplete inhibition by DMSO is the contribution to some extent of other reactive oxygen species to the generation of benzyl radicals. Complete quenching of product **2** by TEMPO indicates that the C-centered benzyl radical is the key reaction intermediate. Benzyl imine would be, then, formed from this radical and would undergo nucleophilic attack by benzylamine, releasing NH_3 and forming *N*-benzylidene benzylamine. In addition, Scheme 2 illustrates the proposed reaction. The fact that the reaction stops upon the removal of the 3DC-4 solid indicates that the chain length of the oxidation process is short, probably because the reaction is taking place inside the pores of the carbon sponge.

CONCLUSIONS

Catalytic data show that the combination of the 3D structure and N, P heteroatom doping is a valuable strategy to develop metal-free carbon-based catalysts for aerobic oxidations. Mechanistic data indicate that the 3D N, P-doped carbon is not acting as an initiator, triggering an oxidation chain mechanism, but as a true heterogeneous catalyst with the occurrence of turnover cycles on the solid. The most efficient N and P-codoped 3D structured carbon with a P and N molar ratio of 0.2 is obtained via pyrolysis at 900 °C of the adduct of phytic acid and chitosan. The 3D N, P-doped carbon materials as powder exhibit large specific surface areas of over 650 $m^2 \times g^{-1}$ and remarkable microporosity of over 0.2 $cm^3 \times g^{-1}$. This N, P-doped carbon catalysts exhibit high stability, being reusable for at least four consecutive uses. Overall, the present results illustrate the potential that the combination of 3D structuring and doping graphene-based materials offers in developing efficient catalysts for aerobic oxidation reactions.

ASSOCIATED CONTENT

Supporting Information

The Supporting Information is available free of charge at https://pubs.acs.org/doi/10.1021/acsomega.1c07179.

Lists of samples and relative percentage of various components of C, N, and P for the samples under study based on XPS deconvolution, Raman and XPS spectra of the samples, and FESEM and HRTEM images of the 3DC samples (PDF)

AUTHOR INFORMATION

Corresponding Authors

Ana Primo − *Instituto Universitario de Tecnología Química, Consejo Superior de Tecnología Química-Universitat Politècnica de Valencia, 46010 Valencia, Spain*; Email: aprimoar@itq.upv.es

Hermenegildo Garcia − *Instituto Universitario de Tecnología Química, Consejo Superior de Tecnología Química-Universitat Politècnica de Valencia, 46010 Valencia, Spain*; orcid.org/0000-0002-9664-493X; Email: hgarcia@upv.es

Authors

Lu Peng − *Instituto Universitario de Tecnología Química, Consejo Superior de Tecnología Química-Universitat Politècnica de Valencia, 46010 Valencia, Spain*

Herme G. Baldovi − *Instituto Universitario de Tecnología Química, Consejo Superior de Tecnología Química-Universitat Politècnica de Valencia, 46010 Valencia, Spain*

https://doi.org/10.1021/acsomega.1c07179
ACS Omega 2022, 7, 11092−11100

Amarajothi Dhakshinamoorthy − *School of Chemistry, Madurai Kamaraj University, 625 021 Madurai, Tamil Nadu, India;* orcid.org/0000-0003-0991-6608

Complete contact information is available at: https://pubs.acs.org/10.1021/acsomega.1c07179

Author Contributions

§L.P. and H.G.B. should be considered as co-first authors since they contributed equally to this work.

Notes

The authors declare no competing financial interest.

■ ACKNOWLEDGMENTS

Financial support by the Spanish Ministry of Science and Innovation (Severo Ochoa 2016 and RTI2018-890237-CO2-R1) and Generalitat Valenciana is gratefully acknowledged. A.P. thanks the Spanish Ministry for a Ramon y Cajal Research associate contract. A.D. is thankful to the University Grants Commission, New Dekhi, for awarding Assistant Professorship through the Faculty Recharge Programme.

■ REFERENCES

(1) Liu, L.; Corma, A. Metal Catalysts for Heterogeneous Catalysis: From Single Atoms to Nanoclusters and Nanoparticles. *Chem. Rev.* **2018**, *118*, 4981−5079.

(2) Zhu, L.; Liu, X.-Q.; Jiang, H.-L.; Sun, L.-B. Metal-Organic Frameworks for Heterogeneous Basic Catalysis. *Chem. Rev.* **2017**, *117*, 8129−8176.

(3) Primo, A.; Parvulescu, V.; Garcia, H. Graphenes as Metal-Free Catalysts with Engineered Active Sites. *J. Phys. Chem. Lett.* **2017**, *8*, 264−278.

(4) Antonietti, M.; Lopez-Salas, N.; Primo, A. Adjusting the Structure and Electronic Properties of Carbons for Metal-Free Carbocatalysis of Organic Transformations. *Adv. Mater.* **2019**, *31*, 1805719.

(5) Primo, A.; Neatu, F.; Florea, M.; Parvulescu, V.; Garcia, H. Graphenes in the Absence of Metals as Carbocatalysts for Selective Acetylene Hydrogenation and Alkene Hydrogenation. *Nat. Commun.* **2014**, *5*, 5291.

(6) Espinosa, J. C.; Navalón, S.; Primo, A.; Moral, M.; Sanz, J. F.; Álvaro, M.; García, H. Graphenes as Efficient Metal-Free Fenton Catalysts. *Chem.—Eur. J.* **2015**, *21*, 11966−11971.

(7) Gu, Q.; Wen, G.; Ding, Y.; Wu, K.-H.; Chen, C.; Su, D. Reduced Graphene Oxide: A Metal-Free Catalyst for Aerobic Oxidative Desulfurization. *Green Chem.* **2017**, *19*, 1175−1181.

(8) Tong, Q.; Liu, Y.; Gao, X.; Fan, Z.; Liu, T.; Li, B.; Su, D.; Wang, Q.; Cheng, M. A Deoximation Method for Deprotection of Ketones and Aldehydes Using a Graphene-Oxide-Based Co-Catalysts System. *Adv. Synth. Catal.* **2019**, *361*, 3137−3145.

(9) Trandafir, M.-M.; Florea, M.; Neaţu, F.; Primo, A.; Parvulescu, V. I.; García, H. Graphene from Alginate Pyrolysis as a Metal-Free Catalyst for Hydrogenation of Nitro Compounds. *ChemSusChem* **2016**, *9*, 1565−1569.

(10) Dhakshinamoorthy, A.; He, J.; Franconetti, A.; Asiri, A. M.; Primo, A.; Garcia, H. Defective Graphene as a Metal-Free Catalyst for Chemoselective Olefin Hydrogenation by Hydrazine. *Catal. Sci. Technol.* **2018**, *8*, 1589−1598.

(11) Duan, X.; Sun, H.; Wang, S. Metal-Free Carbocatalysis in Advanced Oxidation Reactions. *Acc. Chem. Res.* **2018**, *51*, 678−687.

(12) Primo, A.; Puche, M.; Pavel, O. D.; Cojocaru, B.; Tirsoaga, A.; Parvulescu, V.; García, H. Graphene Oxide as a Metal-Free Catalyst for Oxidation of Primary Amines to Nitriles by Hypochlorite. *Chem. Commun.* **2016**, *52*, 1839−1842.

(13) Dreyer, D. R.; Jia, H.-P.; Bielawski, C. W. Graphene Oxide: A Convenient Carbocatalyst for Facilitating Oxidation and Hydration Reactions. *Angew. Chem., Int. Ed.* **2010**, *49*, 6686 S6813/1-S6813/15.

(14) Dreyer, D. R.; Park, S.; Bielawski, C. W.; Ruoff, R. S. The Chemistry of Graphene Oxide. *Chem. Soc. Rev.* **2010**, *39*, 228−240.

(15) Zhao, L.; Sui, X.-L.; Li, J.-L.; Zhang, J.-J.; Zhang, L.-M.; Wang, Z.-B. 3d Hierarchical Pt-Nitrogen-Doped-Graphene-Carbonized Commercially Available Sponge as a Superior Electrocatalyst for Low-Temperature Fuel Cells. *ACS Appl. Mater. Interfaces* **2016**, *8*, 16026−16034.

(16) Niu, J.; Domenech-Carbó, A.; Primo, A.; Garcia, H. Uniform Nanoporous Graphene Sponge from Natural Polysaccharides as a Metal-Free Electrocatalyst for Hydrogen Generation. *RSC Adv.* **2019**, *9*, 99−106.

(17) He, K.; Chen, G.; Zeng, G.; Chen, A.; Huang, Z.; Shi, J.; Huang, T.; Peng, M.; Hu, L. Three-Dimensional Graphene Supported Catalysts for Organic Dyes Degradation. *Appl. Catal., B* **2018**, *228*, 19−28.

(18) Ji, X.; Zhang, X.; Zhang, X. Three-Dimensional Graphene-Based Nanomaterials as Electrocatalysts for Oxygen Reduction Reaction. *J. Nanomater.* **2015**, *2015*, 1−9.

(19) Li, R.; Wei, Z.; Gou, X. Nitrogen and Phosphorus Dual-Doped Graphene/Carbon Nanosheets as Bifunctional Electrocatalysts for Oxygen Redn. And Evolution. *ACS Catal.* **2015**, *5*, 4133−4142.

(20) Zhang, J.; Zhao, Z.; Xia, Z.; Dai, L. A Metal-Free Bifunctional Electrocatalyst for Oxygen Reduction and Oxygen Evolution Reactions. *Nat. Nanotechnol.* **2015**, *10*, 444−452.

(21) Zhang, J.; Qu, L.; Shi, G.; Liu, J.; Chen, J.; Dai, L. N,P-Codoped Carbon Networks as Efficient Metal-Free Bifunctional Catalysts for Oxygen Reduction and Hydrogen Evolution Reactions. *Angew. Chem., Int. Ed.* **2016**, *55*, 2230−2234.

(22) Esteve-Adell, I.; Crapart, B.; Primo, A.; Serp, P.; Garcia, H. Aqueous Phase Reforming of Glycerol Using Doped Graphenes as Metal-Free Catalysts. *Green Chem.* **2017**, *19*, 3061−3068.

(23) Ji, Y.; Shi, Y.; Liu, C.; Zhang, B. Plasma-Regulated N-Doped Carbon Nanotube Arrays for Efficient Electrosynthesis of Syngas with a Wide CO/H 2 Ratio. *Sci. China Mater.* **2020**, *63*, 2351−2357.

(24) Wang, G.; Yu, M.; Feng, X. Carbon Materials for Ion-Intercalation Involved Rechargeable Battery Technologies. *Chem. Soc. Rev.* **2021**, *50*, 2388−2443.

(25) Su, C.; Tandiana, R.; Balapanuru, J.; Tang, W.; Pareek, K.; Nai, C. T.; Hayashi, T.; Loh, K. P. Tandem Catalysis of Amines Using Porous Graphene Oxide. *J. Am. Chem. Soc.* **2015**, *137*, 685−690.

(26) Wu, H.; Su, C.; Tandiana, R.; Liu, C.; Qiu, C.; Bao, Y.; Wu, J. e.; Xu, Y.; Lu, J.; Fan, D.; Loh, K. P. Graphene-Oxide-Catalyzed Direct Ch-Ch-Type Cross-Coupling: The Intrinsic Catalytic Activities of Zigzag Edges. *Angew. Chem., Int. Ed.* **2018**, *57*, 10848−10853.

(27) Peng, L.; Doménech-Carbó, A.; Primo, A.; García, H. 3d Defective Graphenes with Subnanometric Porosity Obtained by Soft-Templating Following Zeolite Procedures. *Nanoscale Adv.* **2019**, *1*, 4827−4833.

(28) Li, J.; He, J. *Alginate-Based Films and Membranes: Preparation, Characterization and Applications*; Scrivener Publishing LLC, 2016; pp 457−489.

(29) Cazón, P.; Velazquez, G.; Ramírez, J. A.; Vázquez, M. Polysaccharide-Based Films and Coatings for Food Packaging: A Review. *Food Hydrocolloids* **2017**, *68*, 136−148.

(30) Kakizaki, M.; Shoji, T.; Tsutsumi, A.; Hideshima, T. Filmogenic Properties of Chitin/Chitosan. *Molecular Motion and Dielectric Relaxation in Chitin and Acyl chitins*; Plenum, 1986; pp 398−402.

(31) Primo, A.; Atienzar, P.; Sanchez, E.; Delgado, J. M.; García, H. From Biomass Wastes to Large-Area, High-Quality, N-Doped Graphene: Catalyst-Free Carbonization of Chitosan Coatings on Arbitrary Substrates. *Chem. Commun.* **2012**, *48*, 9254−9256.

(32) Primo, A.; Forneli, A.; Corma, A.; García, H. From Biomass Wastes to Highly Efficient Co2 Adsorbents: Graphitisation of Chitosan and Alginate Biopolymers. *ChemSusChem* **2012**, *5*, 2207−2214.

(33) Albero, J.; Vidal, A.; Migani, A.; Concepción, P.; Blancafort, L.; García, H. Phosphorus-Doped Graphene as a Metal-Free Material for Thermochemical Water Reforming at Unusually Mild Conditions. *ACS Sustainable Chem. Eng.* **2019**, *7*, 838−846.

(34) Lavorato, C.; Primo, A.; Molinari, R.; Garcia, H. N-Doped Graphene Derived from Biomass as a Visible-Light Photocatalyst for Hydrogen Generation from Water/Methanol Mixtures. *Chem.—Eur. J.* **2014**, *20*, 187−194.
(35) Jurca, B.; Bucur, C.; Primo, A.; Concepcion, P.; Parvulescu, V. I.; Garcia, H. N-Doped Defective Graphene from Biomass as Catalyst for CO2 Hydrogenation to Methane. *ChemCatChem* **2019**, *11*, 985−990.

https://doi.org/10.1021/acsomega.1c07179
ACS Omega 2022, 7, 11092−11100